Electronic Supplementary Material (ESI) for RSC Advances.
This journal is © The Royal Society of Chemistry 2015

Electronic pH switching of DNA triplex reactions

Gabriel Antonio S. Minero, Patrick F. Wagler, Alaa A. Oughli, and John S. McCaskill

Ruhr-Universität Bochum

Supplementary Information

Design of the pH switchable DNA complexes

DNA sequences employed in the design of the switchable DNA structures are listed in the Table 1. The structures of the triplexes forming under low pH conditions are shown below (Fig. S1). The two-colour detection for triplex complexes is illustrated in (A). Cycling of DNA conformations via pH was followed by reversible changes of fluorescence associated with binding and release of the quencher strand (B). The fluorescent labels Alexa488 (blue) as well as Alexa647 (red), and the quencher BHQ-3 were commercially synthesized as well as attached to DNA in standard oligonucleotide synthesis (IBA).

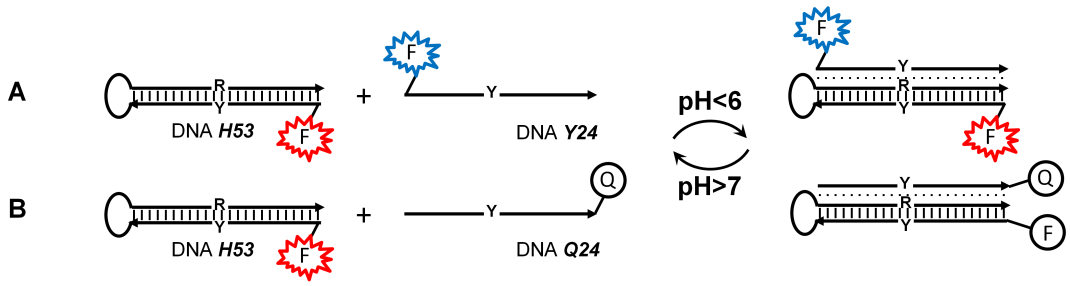

Fig. S1. Schematic illustration of DNA complexes formed between homopyrimidine (Y) and homopurine (R) DNA sequences (Table 1). Binding of the third strand (ssY24) to the hairpin and release are illustrated at pH<6 and at pH>7, respectively. A) Two-colour fluorescently labelled DNA was designed for separation of DNA complexes and their analysis via CGE (Fig. 3). The fluorescence labels are Alexa647 and Alexa488 attached to the 5'-ends of hairpin DNA H53 and ssY24, respectively. B) The pH-dependent equilibrium was studied further using the fluorescence quenching technique. For this, the third strand carried a Black Hole Quencher moiety (BHQ-3) at its 3'-end, which can quench Alexa647 at the 5'-end of the hairpin due to antiparallel organization of the pyrimidine strands in triplex DNA at pH<6.

Spectroscopic analysis of triplex DNA and its conformational transitions

As DNA hybridization structures melt, nucleic acid bases became unstacked, causing an increase of absorbance at 260nm (hyperchromic effect) in UV absorption analysis. The duplex and third strand displayed one transition at pH 7.5 and two transitions at pH below 6.0 (Fig. S2). The transition of duplex to single strands at high pH (grey line, Fig. S2, A and B) revealed the same value of hyperchromism as the second transition at low pH (broken as well as unbroken lines, Fig. S2, A and B). As a consequence, the first melting transition at low pH could be assigned as the transition of triplex to duplex. The second transition is overlaid with the first transition, giving the appearance of a higher weight to the triplex to duplex transition. This was separately checked via circular dichroism (CD) measurements (Fig. S2, C).

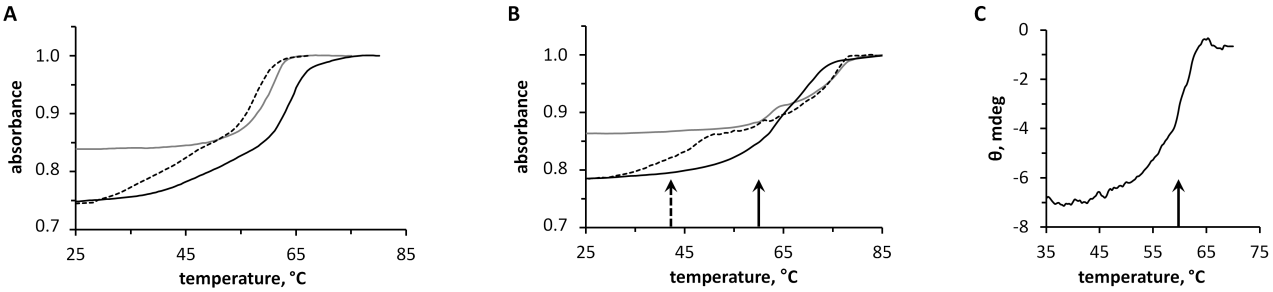

Fig. S2. DNA UV melting curves for trimolecular and bimolecular triplex systems. Temperature dependence of DNA transitions in systems Y:R:Y (A) and H:Y (B) in 10 mM phosphate buffer at pH 7.5, 6.0 and 5.0 at the increasing temperature 0.5°/min. Triplex to duplex transition is overlaid in (B) with melting of hairpin DNA, both Tm are within the grey box. C) Melting behaviour of the system H:Y as well as triplex Tm ca. 60 °C (pH 5.0) measured via CD at 213 nm. DNA H:Y of concentration 1 µm (A,B) as well as 2 µM (C) was placed in a quartz cuvette with 10 mm optical path length. Melting profiles of DNA were concentration independent (1-5 µM). The phosphate buffer employed held the system to pH 5.0 (black unbroken line), 6.0 (black broken line) and 7.5 (grey line). The arrows represent the triplex to duplex transition at pH 6.0 (broken in B) as well as the triplex to coil transition at pH 5.0 (unbroken in B and C).

The CD spectra in both systems, Y:R:Y and H:Y, showed large positive 276 nm, small negative 242 nm and small positive 220 nm bands, confirming at pH 7.5 the presence of B-form double-stranded DNA (Fig. S3, A and B, respectively). As the pH was reduced, a red shift of the bands and loss of the 220 nm band were observed. By pH 5.0, major changes in the CD spectrum had occurred, to exhibit positive 280 nm, negative 248 nm and negative 213 nm bands. The CD spectra of system HY were very similar to those of system Y:R:Y, both are in agreement with literature data. [1]

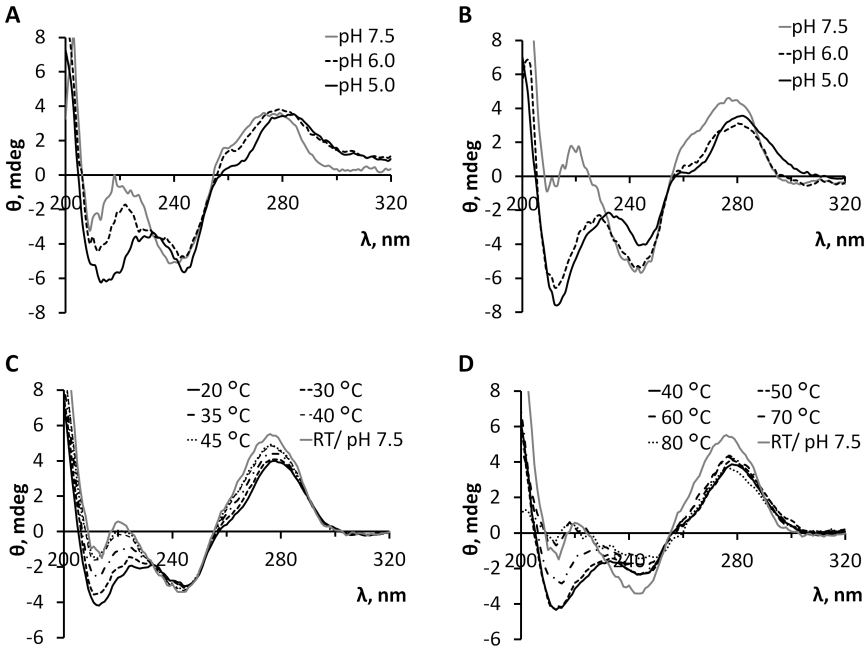

Fig. S3. CD profiles of triplex complexes of DNA. Verification of temperature dependence of formation of hairpin DNA triplex by circular dichroism. A) Fully intermolecular Y:R:Y system at 23 °C at various pH. At pH 6.0, an isothermal transition from triplex to duplex was observed. B) Hairpin:single strand, H:Y, system at 23 °C at various pH. C) CD profiles of the H:Y system at pH 6.0. The CD spectrum at 45 °C is virtually identical to the CD spectrum at high pH (23 °C). D) CD profiles for the H:Y system at pH 5.0. All profiles are obtained at constant temperatures as described in Materials and Methods. The 1 µM samples in (A) and (B) were placed in a 10 mm path length quartz cuvette, while the 5 µM samples in (C) and (D) had a 2 mm optical path. The high pH spectrum (RT/7.5) is a reference in (C) and (D).

For the main system of study, H:Y**,** we then followed CD spectra at temperatures 20°-90°C at low pH and at 20°C at high pH (Fig. S3, C and D). At pH 6.0 we observed the appearance of a positive 220 nm band as well as blue shift of 278 nm and 245 bands with increasing temperature that resulted in a spectrum which, at 45°C, is virtually identical to the form of spectrum at pH 7.5. At pH 5.0, no difference between spectra collected in the range 20-40°C was observed. A 220 nm band appeared at 60°C. At temperatures higher than 70°C, the CD spectra were consistent with thermally disordered single strands. However, no spectrum identical to that at pH 7.5 was observed, which clearly showed the difference between melting behaviour at pH 5.0 and 6.0: one and two phase transitions respectively. Although the triplex to duplex transitions in UV show complex behaviour, the triplex to duplex/single strands transition could be identified by CD at a melting temperature at 60-63 °C (see also Fig. S2, C).

The melting temperature of the hairpin DNA **H24** (T_m = 74 °C, Fig. S2, B) was higher than that for the **Y:R** duplex (T_m = 58 °C, Fig. S2, A), when measured in the standard buffer at pH 7.5, as is expected for a unimolecular transition. Unexpectedly, there was only a single transition monitored in the mixture of DNA strands **H24** and **Y** at pH 5.0 (T_m ca. 60-65 °C). A thorough analysis via CD measurements (see Fig. S3) demonstrated that triplex DNA was formed but that the transition of triplex to duplex overlaid the second transition to ss DNA. One can conclude that the T_m of triplex was increased from ca. 43-45 °C (Y:R:Y) to ca. 60-63 °C (H:Y) at pH 5.0.

Capillary Gel Electrophoresis (CGE) conformational analysis

We employed CGE as a tool for monitoring transitions in triplex DNA systems, first those involving ts Y:R:Y at different pH (Fig. 3, Fig. S4). In the first instance, the system Y:R*:Y was labelled with Alexa488 on the purine strand (Fig. S4, A), showing three peaks with the third one broader that could imply partial release of Y strand from the triplex. The longer separation time contributed to significant broadening of the third peak that had a tendency to split one triplex peak into two peaks. The CGE traces (10-15 min) revealed a dynamic equilibrium between bound and unbound strands in the Y:R:Y system at pH 5.

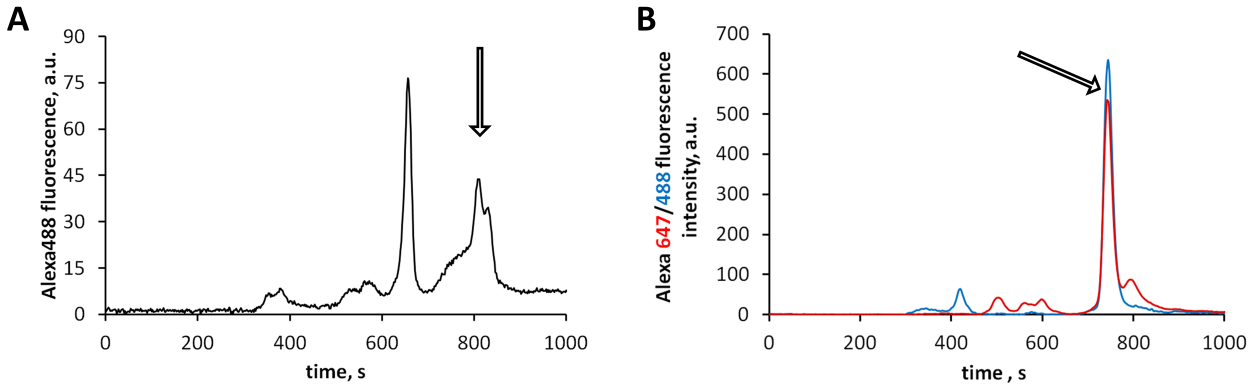

Fig. S4. CGE separation of the annealed Y:R:Y DNA complex (A) and H:Y DNA complex (B) in Pluronic block-copolymer matrix. A) One colour (Alexa488) detection of the pre-annealed fully intermolecular triplex (current 35 ± 3 µA). B) Two colour (Alexa647, red, and Alexa488, blue) detection of the pre-annealed looped triplex (current 41 ± 4 µA). Separation media: 25 % Pluronic in 50 mM tris-acetate buffer. See Materials and Methods for more details. The triplex structure was identified as shown by the arrows, with the aid of multicolour labelling.

To get a more clear attribution of peaks to particular states of DNA, we also studied the **H:Y** system using two-colour detection with Alexa647 ds **H24** and Alexa488 ss **Y24** (Fig. S4, B). The stability of triplex DNA was checked separately by UV and CD (Figs. S2 and S3) measurements. The expected increase in triplex stability for the bimolecular system (compared with termolecular) was also observed in the CGE experiments.

Preparation of pMBQ modified surfaces

We first immobilized the pMBQ redox system to the simple open layer electrode microarray. The modification steps are shown for disk electrode as well as microchip. Immobilization of the pMBQ to a gold surface via the thiol group was followed by electropolymerization of pMBQ to make polymer chains (Fig. S5, A). The new electrochemical properties of the modified surface were studied using the cyclic voltammetry (CV) method. The reduction peak of the pMBQ layer appeared clearly at a potential near -200 mV (B). The stability of the pMBQ-modified electrode was established by the linearity of the current vs. scan rate plot.

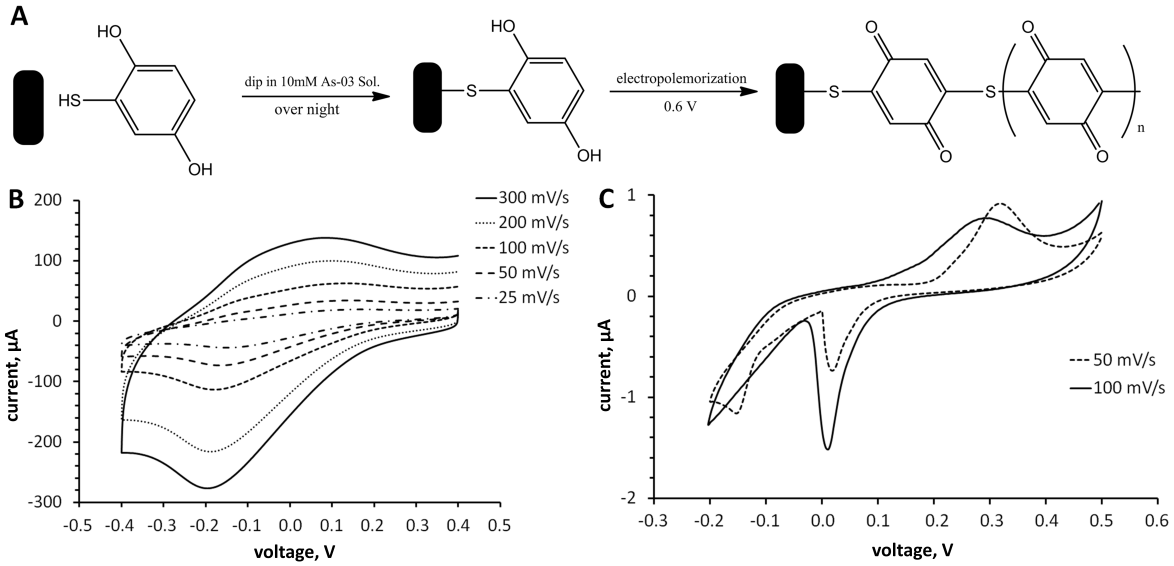

Fig. S5. Modification of disc gold electrode by pMBQ (for details see [2]). A) Schematic illustration of pMBQ synthesis on the gold surface. B) CV of pMBQ-modified gold electrode. C) CV of pMBQ-modified gold microelectrodes on a chip.

The same modification principle was applied to the microchip, which contains 3000 gold microelectrodes [3]. Since the modification was taking place over the whole surface of the microchip, the gold microelectrodes had to be divided into working, reference and counter electrodes when connected to a conventional potentiostat (µ-Autolab III FRA, Deutsche Metrohm GmbH & Co. KG). CV of the modified microelectrodes was performed after the modification & electropolymerization steps. In contrast to the case of the disk electrode, the cyclic voltammetry of the microchip showed some deviations as expected from the use of a subset of gold electrodes as pseudo-reference electrodes (Fig. S5, C).

Electrochemical pH cycles on a chip

The prepared pMBQ-modified microelectrodes displayed fast pH changes (12 - 30 s) in the range 5.6 - 7.5 (see Fig. 4). They were applied to the **H:Q** system (Fig. S6). At the cathode pH increased due to the redox reaction of pMBQ, and triplex was dissociated into free DNA **H** and **Q**. This resulted in a fluorescence enhancement over 2 - 2.5 min as well as a following gradual decrease of the signal due to repulsion of DNA from the microelectrodes. This finding is in the good agreement with the bulk cycles on triplex DNA, where release of the quencher strand took 3 min and more over negative microelectrodes (see Fig. 7C). The sharp fall of the fluorescence signal over anodic microelectrodes was considered to be caused by the pH-mediated **H:Q** association, self-quenching (due to high DNA concentration and exceeding the 50 nm threshold of FRET quenching), by non-radiative emission in the vicinity of gold surface (2 nm, SPR), and possibly also by quinones (nine step redox reaction of benzoquinone). Relaxation of potential (to tristate, high Z) was accompanied by a sharp fluorescence peak followed by fluorescence decrease due to diffusion

of DNA away from the monitored region of interest. This phenomenon occurred over multiple voltage cycles, two of them are shown in the Fig. S6. In the later cycles there was a reproducible loss of fluorescence observed.

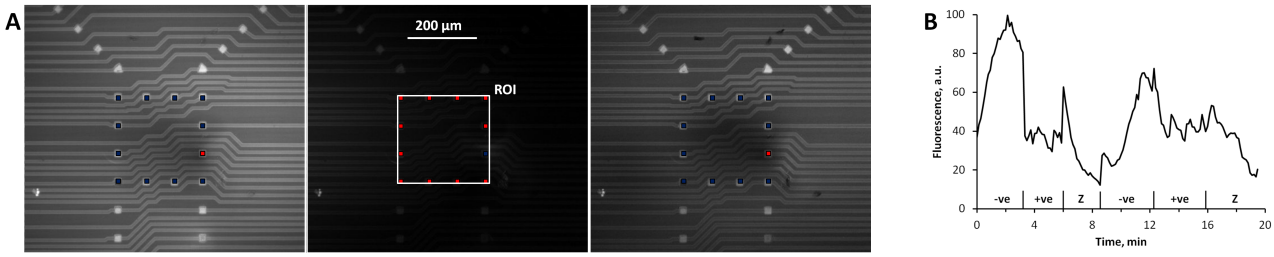

Fig. S6. Conformational cycles of triplex between bound **H:Q** and unbound **H** and **Q** by pMBQ-modified gold microelectrodes on a chip. A) Fluorescence images of the system placed in a thin film (30 µm) over the chip, acquired at the fluorescence microscope (10-fold magnification, 1 s exposure time) while switching the electrode configuration. The electrodes are represented by coloured squares, red and blue, for positive and negative potential, respectively. The ROI square represents the detection area, at which fluorescence intensity was calculated via ng_biopro. B) Plot of the fluorescence intensity obtained from the raw images, such as illustrated in A. The electrode configuration was switched between positive (+ve), negative (-ve) as well tri-state (Z) at time points indicated with the bars. Two cycles of the electrode configuration switching are shown. The curve followed the same tendency as in the microfluidic measurements.

We used a phosphate buffer in all electrochemical experiments in order to support quick and stable pH changes. Optimal conditions for stable pH cycles were achieved furthermore in this work in the system of 30 mM quinhydrone (QH) and 50 mM phosphate buffer. The buffer concentration used in the mixtures to support pH changes varied from 1 mM to 100 mM, since the amount of the phosphates in the system played a crucial role in the pH changes achieved. At a phosphate concentration below 5 mM, fluorescence of SNARF-4F was quenched over long distances upstream as well as downstream of positive electrodes, which is most likely associated with a pH lower than the pKa of $H_2PO_4^-$. As the buffer concentration increased, the extent of SNARF quenching was more localized to the area of positive electrodes. Here one of the less stable examples of pH cycling is shown (Fig. S7) for comparison.

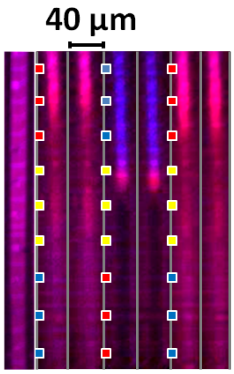

Fig. S7. Sharp changes of pH in 8mM phosphate buffer. A sharp transition of pH occurred between the two areas controlled by negative and positive microelectrodes. Values of pH were assigned based on the ratios of SNARF-4F fluorescence intensities obtained at two emission wavelengths I_{700}/I_{384} as in M&M. Successive images of a single channel were displayed over a period of 6 minutes. Initial pH was 6 (the first frame) and then pH was oscillated between ca. 4 (or below) and 7 via alternating polarity of the electrodes (as schematically shown by red and blue squares). The colour scheme used to report pH is shown in Fig. 2.

At buffer concentration 5-10 mM, there was a band of shorter wavelength SNARF emission (585 nm, pink colour, see Fig. S7) reporting pH *ca.* 5.5. That area of exhausted buffer capacity was observed on the boundary between the quenched fluorescence over positive microelectrodes and its longer wavelength emission (700 nm, blue colour) over negative microelectrodes. The sharp transition of pH from 6.8 to a value below 4 is in good agreement with the finite buffer capacity of the phosphate buffer (see also remote switching of pH in Fig. 6).

In addition, the voltage level used for digital switching of microelectrodes also played a crucial role in achieving stable reproducible pH cycling. At higher amplitude voltage (2.5V) the analysis of pH cycles revealed a gradual shift of periodic pH values towards more acidic pH in 50 mM buffer (Fig. 5). In contrast to the 2.5 V response, at 1.8 V constant reproducible pH cycles were obtained without drift (Fig. S8).

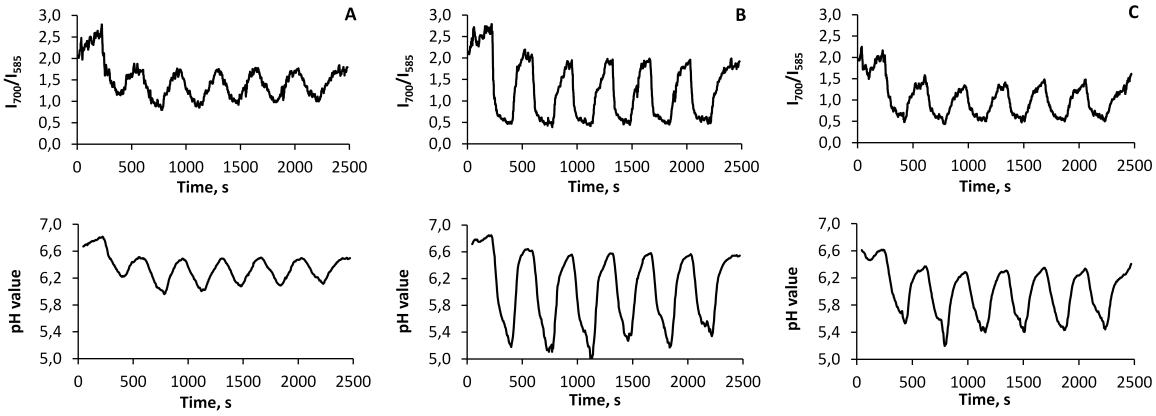

Fig. S8. Time patterns of pH in a microfluidic channel cycled via digital microelectrode potentials (at 0 and 1.8V) detected with SNARF-4F. Plots indicate values of ratiometric I700/I585 fluorescence intensities (ex. 488 nm) as in Materials and Methods. Three different ROIs (40x40 µm, 50x50 pixel), placed in the microchannel over the microelectrodes (as in Fig. 5), were used to record oscillations of pH patterns: A) lateral to driving electrodes, B) and C) in between in between electrodes. Stable pH oscillations were observed.

References

[1] Plum G E and Breslauer K J 1995 Thermodynamics of an intramolecular DNA triple helix: a calorimetric and spectroscopic study of the pH and salt dependence of thermally induced structural transitions *Journal Of Molecular Biology* **248(3)** 679-95

[2] Oughli A A, Electrochemically Stimulated pH Changes by pMBQ-modified Microelectrodes, in practical thesis. 2012, Ruhr-University Bochum.

[3] Wagler P F, et al. 2012 Field programmable chemistry: integrated chemical and electronic processing of informational molecules towards electronic chemical cells. *Bio Systems* **109(1)** 2-17